Click Here for Full Article

Stress change and effective friction coefficient along the Sumatra-Andaman-Sagaing fault system after the 26 December 2004 (M_w = 9.2) and the 28 March 2005 (M_w = 8.7) earthquakes

R. Cattin

Laboratoire de Géologie, UMR8538, Ecole Normale Supérieure, CNRS, Paris, France (cattin@geologie.ens.fr)

Now at Laboratoire Géosciences Montpellier, Université Montpellier 2, CNRS, CC 60, Place Eugène Bataillon, F-34095 Montpellier, France

N. Chamot-Rooke, M. Pubellier, A. Rabaute, M. Delescluse, C. Vigny, L. Fleitout, and P. Dubernet

Laboratoire de Géologie, UMR8538, Ecole Normale Supérieure, CNRS, Paris, France

[1] The 2004 Aceh and 2005 Nias events are the two greatest earthquakes of the past 40 years with a total rupture of 1700 km long and a coseismic slip reaching up to 25 m. These two earthquakes have caused large stress perturbations which significantly altered seismic activity in the Sumatra-Andaman region. Using both detailed mapping of failure planes and various slip distributions, we calculate this stress change along the Sumatra-Andaman-Sagaing fault system from central Sumatra to southern Myanmar. The static Coulomb stress change ΔCFF and the observed seismic activity are in very good agreement with a Coulomb index $\sim$ 20% greater than the one obtained for random events. Compared to previous studies, this high Coulomb Index confirms two important issues on the use of static stress change criterion: unsuited to study near-field aftershocks and only relevant for aftershocks analysis on large and mature faults at a time scale of several months. The calculated ΔCFF distribution suggests that the 2004 and 2005 earthquakes inhibit failure on the North Andaman rift and on the Sagaing fault, while failure is encouraged along the transform Andaman zone, the central Andaman rift, the West Andaman fault, the Sumatra fault system, and the offshore thrust faults west of Sumatra Island. The maximum value of $\sim$15–20 bar (1.5–2 MPa) for ΔCFF is reached in the northern part of the Sumatra fault system. This high value together with the lack of major earthquake in the last 170 years result in a high seismic hazard for this region. Our results are also consistent with temporal evolution of both earthquakes' location and focal mechanism prior to and after the events. In particular, we explain the occurrence and the mechanism of seismic swarms observed in the central Andaman rift and along the west Andaman fault. Finally, our calculations reveal that the seismicity in the Andaman rift zone can only be explained if $\mu' > 0.5$. This result leads to two end-member models: one with a constant and high fault friction and one with spatial variations, for which friction may depend on either the nature of the lithosphere (oceanic versus continental) or the fault type.

Components: 8810 words, 17 figures, 1 table.

Keywords: Sumatra; stress triggering; friction.

1. Introduction

[2] The Sunda-Andaman megathrust is one of the most seismically active structures in the world, with great earthquakes often followed by destructive tsunamis. Seismicity results from the subduction of the India and Australia plates beneath the Eurasia plate, which includes the Andaman microplate and Sunda subplate in Southeast Asia (Figure 1). The convergence rate decreases northward from ~56 mm/a in the Sunda Strait to ~37 mm/a offshore south Myanmar [*Socquet et al.*, 2006; *Delescluse and Chamot-Rooke*, 2007]. Because of the large north component of the India-Australia plate motion, convergence becomes increasingly oblique from south to north along the Sumatra and Andaman trenches, which results in the activation of large-scale shear structures including the Sagaing fault, the Andaman rift zone, the West Andaman fault and the Sumatra fault system (called the Sagaing-Andaman-Sumatra fault system hereinafter).

[3] Over the last century and before 2004, most of the large subduction events occurred off the Sumatra island and, with the exception of the 1941 event, no major earthquake had been recorded to the north between Sumatra and Myanmar (Figure 1). Unfortunately, the 26 December 2004 M_w 9.2 Aceh earthquake released a large amount of accumulated strain on this northern portion of the megathrust, which caused one of the worst natural disasters in modern history. This giant rupture apparently triggered three months later a second great earthquake, the M_w 8.7 Nias event, along the Sunda subduction zone [*Nalbant et al.*, 2005].

[4] It has been observed for more than a century that aftershocks occur in the vicinity of the main shock rupture zone [*Omori*, 1894] and it is now widely accepted that there is a positive correlation between the coseismic stress change and the location of the subsequent events [e.g., *Das and Scholz*, 1981; *Stein and Lisowski*, 1983; *Hill*, 1993; *Harris*, 1998; *Steacy et al.*, 2005]. It thus seems natural to investigate the stress changes associated with the 2004 Aceh and the 2005 Nias earthquakes in order to evaluate the seismic hazard in the Sumatra-Andaman region. Under Coulomb failure theory, previous studies have mainly focused on the stress change on the Sunda thrust as well as on the Sumatra fault system [e.g., *McCloskey et al.*, 2005; *Nalbant et al.*, 2005; *Gahalaut*, 2005; *Pollitz et al.*, 2006]. Surprisingly little is known about the state of stress on the Andaman thrust [*Mignan et al.*, 2006] and there is no published study of the normal and strike-slip faults in the region between Sumatra and Myanmar as well as the offshore structures in the west of the Sumatra Island.

[5] Here we investigate the stress change on these structures using detailed 3D description of fault geometry and a wide set of slip distribution recently proposed for the 2004 Aceh and the 2005 Nias earthquakes [*Vigny et al.*, 2005; *Briggs et al.*, 2006; *Chlieh et al.*, 2007; *Rhie et al.*, 2007; *Fujii and Satake*, 2007; *Banerjee et al.*, 2007; C. Ji, Preliminary result of the Mar 28, 2005 Mw 8.68 Nias Earthquake, 2005, available at http://www.geol.ucsb.edu/faculty/ji/big_earthquakes/home.html]. Using the earthquakes relocated by *Engdahl et al.* [2007] in a time span of 2 years after the 2004 Aceh earthquake, we discuss the effect of both Aceh and Nias earthquakes on the Coulomb stress change distribution along the Sagaing-Andaman-Sumatra fault system. Finally, assuming that the static Coulomb stress is a reliable criterion to describe the location of seismicity after a major earthquake, we assess the distribution of field-scale friction along these major structures.

2. Method and Data

2.1. Coulomb Stress Change Calculation

[6] A common criterion for aftershocks occurrence is the static Coulomb stress change [e.g., *King et*
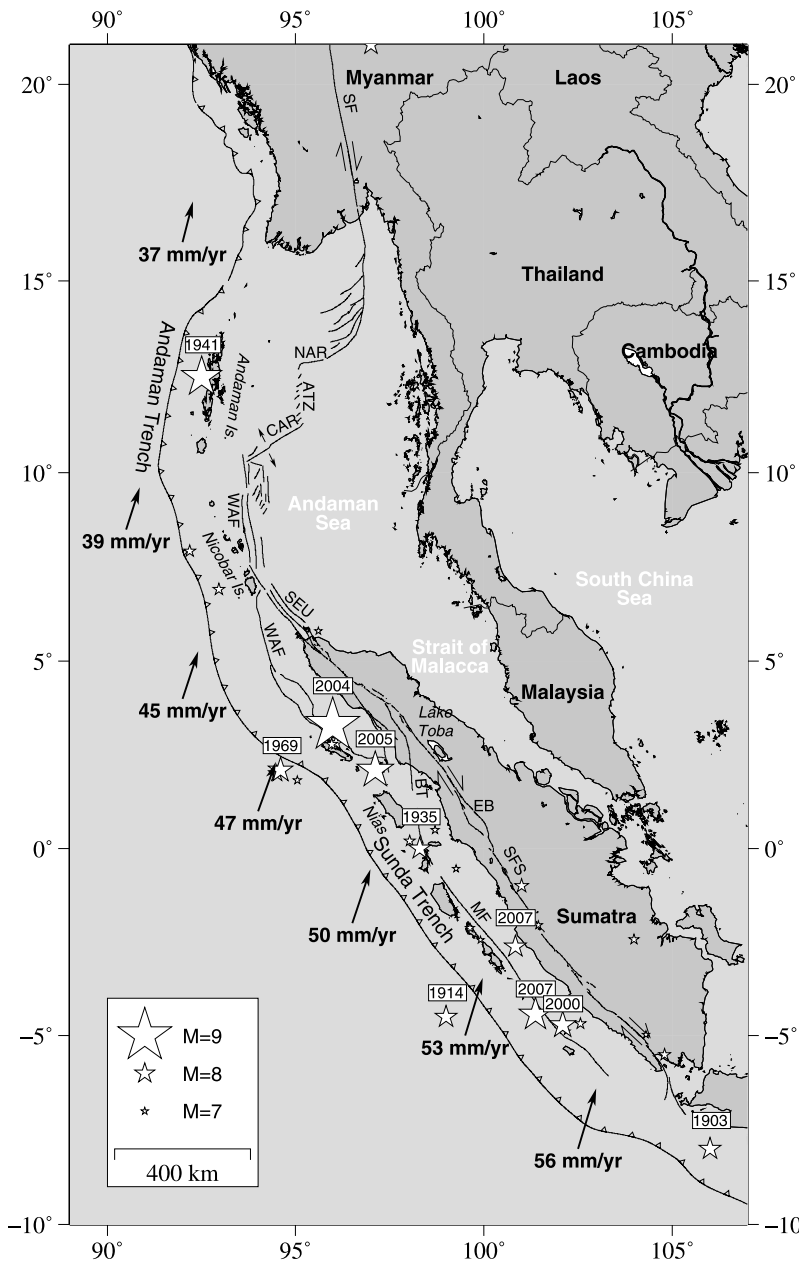
Figure 1. Simplified tectonic map showing the major faults of the Andaman-Sumatra region. SF, Sagaing Fault; NAR, North Andaman Rift; ATZ, Andaman Transform Zone; CAR, Central Andaman Rift; WAF, West Andaman Fault; SEU, Seuliman Fault; BT, Batee fault; EB, Equatorial Bifurcation; SFS, Sumatra Fault System; MF, Mentawai Fault. White stars indicate the location of the largest earthquakes of the last century. Black arrows give the plate velocities India/Australia relative to Sunda [*Socquet et al.*, 2006; *Delescluse and Chamot-Rooke*, 2007].

al., 1994; *Stein*, 1999],

$$\Delta CFF = \Delta\tau - \mu(\Delta\sigma_n - \Delta P_p), \qquad (1)$$

which states that an increase of ΔCFF could promote failures nearby rupture zone. Here $\Delta\tau$ is the static shear stress change on the failure planes (positive in the direction of fault slip), $\Delta\sigma_n$ the static normal stress change (positive if the fault is clamped), ΔP_p the change in pore fluid pressure (positive in extension), and μ the friction coefficient.

[7] According to *Rice and Cleary* [1976] the pore pressure change in an undrained poroelastic medium is related to the mean stress change ΔP by

$$\Delta P_p = B\Delta P = B\Delta\sigma_{ii}/3 \qquad (2)$$

Table 1. References of Coseismic Slip Distributions Used in This Study

Nias Earthquake[a]	Aceh Earthquake[b]		
	Chlieh et al. [2007]	*Rhie et al.* [2007]	*Fujii and Satake* [2007]
Briggs et al. [2006]	model 1	model 4	model 7
C. Ji (Preliminary result of the Mar 28, 2005 Mw 8.68 Nias Earthquake, 2005, available at http://www.geol. ucsb.edu/faculty/ji/big_earthquakes/home.html)	model 2	model 5	model 8
Banerjee et al. [2007]	model 3	model 6	model 9

[a] See Figure 3.
[b] See Figure 2.

where σ_{ii} indicates summation over the diagonal elements of the stress tensor and B is the Skempton coefficient. Using equations (1) and (2) the Coulomb stress change is given by

$$\Delta CFF = \Delta\tau - \mu(\Delta\sigma_n - B\Delta\sigma_{ii}/3). \qquad (3)$$

[8] Assuming that the change in the mean stress is proportional to the normal stress change [see *Cocco and Rice*, 2002, and references therein]

$$B\Delta\sigma_{ii}/3 = B'\Delta\sigma_n, \qquad (4)$$

equation (3) is commonly replaced by

$$\Delta CFF = \Delta\tau - \mu'\Delta\sigma_n, \qquad (5)$$

where $\mu' = \mu(1 - B')$ is the effective friction coefficient.

[9] Here we describe the previously published rupture zones by a surface of displacement discontinuities in isotropic homogeneous half space. Each dislocation induces a 3-D stress change field, which is estimated from the analytical solution of *Okada* [1992] using a Poisson ratio $v = 0.25$ and a Young modulus $E = 75$ GPa. The calculation of the static Coulomb stress change thus requires a well-constrained coseismic rupture (geometry and slip distribution) to estimate the static stress change within the crust, a good knowledge of the failure planes to calculate both normal and shear stress change, and information on both friction and poroelastic properties in the area of interest.

2.2. Rupture Zone and Slip Distribution

2.2.1. Geometry

[10] The geometry of rupture zones is usually inferred from geological studies, seismic profile or background seismicity. For the 2004 Aceh and the 2005 Nias earthquakes the geometry of the rupture zone is not well constrained. It is mainly delineated from the geometry of the Andaman-Sunda trench and from relocated seismicity [*Engdahl et al.*, 1998], Global CMT of aftershocks and background earthquakes. This leads to slight differences between the proposed models. For instance, *Chlieh et al.* [2007] and *Rhie et al.* [2007] consider a northward increase in dip angle from ~11° to ~18°, whereas *Fujii and Satake* [2007] used a constant dip angle of 10°. Here, to overcome this issue several geometries with various degrees of complexity will be tested (see Table 1).

2.2.2. Slip Distribution

[11] The proposed slip distributions of the 2004 Aceh and the 2005 Nias earthquakes have been obtained from the inversion of various data sets, which include GPS displacements, coral observations, long-period teleseismic data, tide gauge records and satellite altimetry measurements. Here, we test three different slip distributions for the 2004 Aceh earthquake (Figure 2) and three for the 2005 Nias earthquake (Figure 3). Note that we study the seismicity in time periods of three months and 2 years after the 2004 Aceh earthquake. We thus favor models that include afterslip. For instance, we use the slip distribution of model G-M9.22 proposed by *Chlieh et al.* [2007], which represents the motion due to the earthquake and 30 days of postseismic deformation.

[12] Altogether the tested slip distributions show common features: for the 2004 Aceh earthquake, (1) the rupture is ~1300 km long, (2) the maximum slip is ~25 m, and (3) the high-slip patch is centered 50 km northwest of the epicenter. For the 2005 Nias earthquake, (1) the rupture is ~400 km long, (2) the maximum slip is ~10 m, and (3) the depth of the high-slip patch is ~30 km.

[13] However, these slip distributions are quite different in detail. Inversion of tide gauge and satellite data [*Fujii and Satake*, 2007] provides for the Aceh rupture low slip in the Nicobar Island
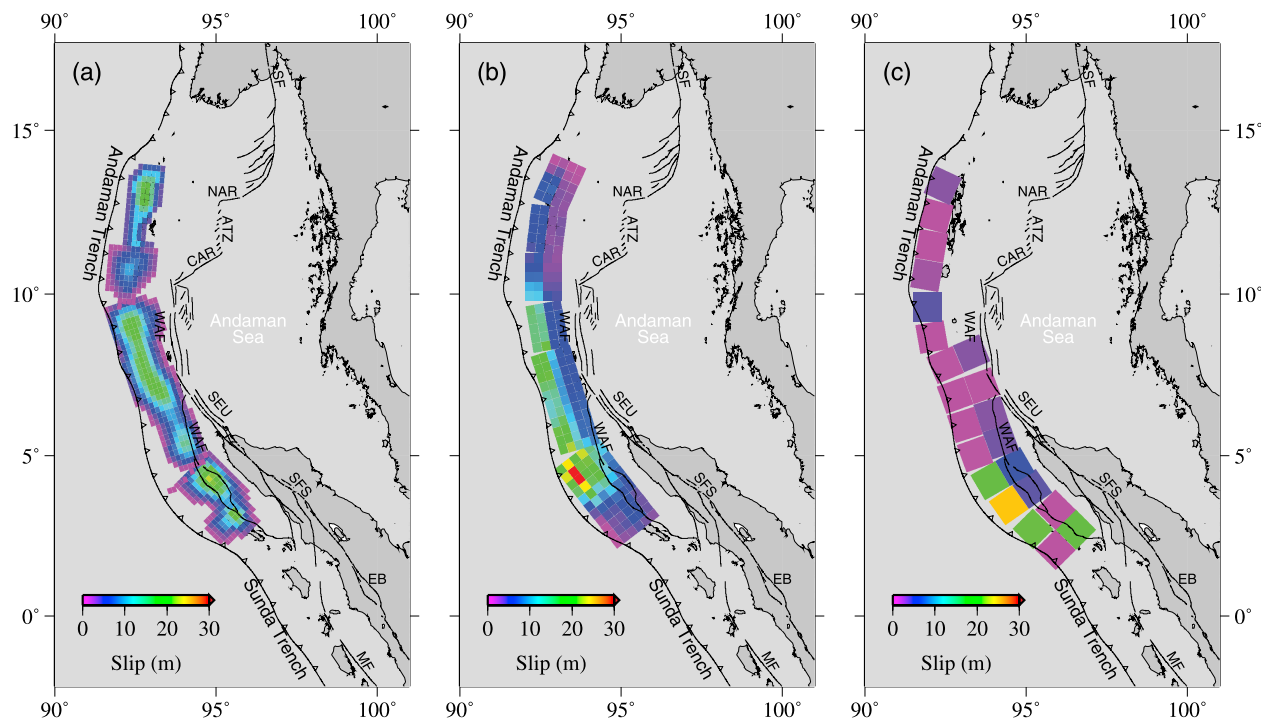
Figure 2. Coseismic slip distribution of the 26 December 2004 Aceh earthquake inferred for different data sets. See Figure 1 for fault labels. (a) Inversion of continuous and campaign GPS measurements [*Chlieh et al.*, 2007]. (b) Joint inversion of GPS and long-period teleseismic data [*Rhie et al.*, 2007]. (c) Joint inversion of tide gauge data and satellite altimetry measurements [*Fujii and Satake*, 2007].
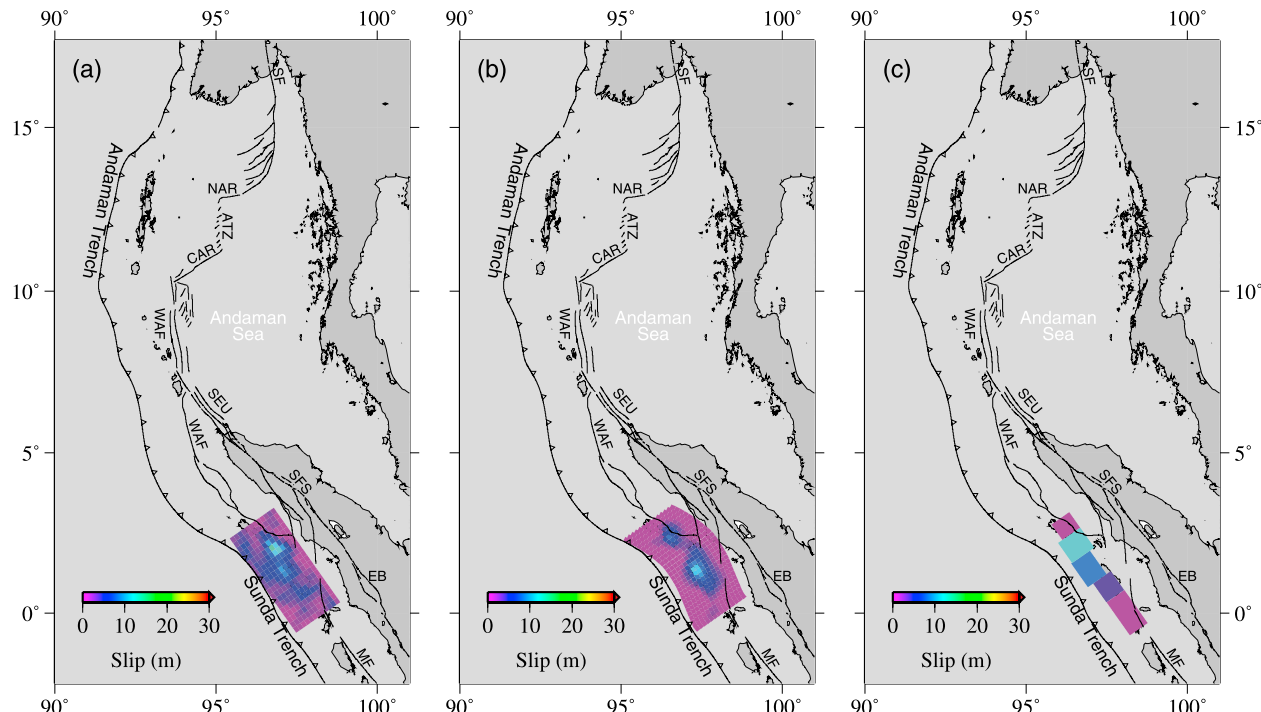
Figure 3. Coseismic slip distribution recently proposed for the 28 March 2005 Nias earthquake. See Figure 1 for fault labels. (a) Joint inversion of GPS and coral data [*Briggs et al.*, 2006]. (b) Inversion of seismic data (C. Ji, Preliminary result of the Mar 28, 2005 Mw 8.68 Nias Earthquake, 2005, available at http://www.geol.ucsb.edu/faculty/ji/big_earthquakes/home.html). (c) Inversion of GPS data [*Banerjee et al.*, 2007].

region, which appears inconsistent with the inversion of GPS and long-period teleseismic data [*Chlieh et al.*, 2007; *Rhie et al.*, 2007]. The extent of the Aceh rupture far to the north is also still in debate [*Vigny et al.*, 2005]. Furthermore for the Nias rupture slip distribution including coral data [*Briggs et al.*, 2006] has a second high-slip patch, which is not obtained with the other data sets [*Banerjee et al.*, 2007; C. Ji, Preliminary result of the Mar 28, 2005 Mw 8.68 Nias Earthquake, 2005, available at http://www.geol.ucsb.edu/faculty/ji/big_earthquakes/home.html]. Postseismic displacements and slightly different rupture geometry may explain some of these discrepancies. Another explanation is the nonuniqueness of this type of source inversion. As previously noted by *Arnadottir and Segall* [1994], *Sagiya and Thatcher* [1999], and *Loevenbruck et al.* [2004] these discrepancies may be associated with the sharp decrease in the slip resolution with distance between rupture and observations in spite of high-quality inverted data. In the following, we assess the effect of the assumed model on the calculated Coulomb stress change after the Aceh and the Nias earthquakes by testing all the combinations of slip distribution proposed for these two events (see Table 1).

2.3. Constraints on Failure Plane Geometry

[14] Following *McCloskey et al.* [2003], we assume here that aftershocks failure planes orientation is mainly controlled by geological structures rather than the coseismic and the regional stress field. Thus, in contrast with most of the common approaches [e.g., *King et al.*, 1994; *Ma et al.*, 2005], the planes optimally oriented for failure mainly derived from regional stress field are not used in our calculation. We favor failure planes orientation controlled by geological fault planes.

[15] Our method to define these orientations of potential failures planes can be summarized by the following steps:

[16] 1. We extracted detailed information from published studies [e.g., *Beaudry and Moore*, 1985; *Diament et al.*, 1992; *Matson and Moore*, 1992; *Kemal*, 1993; *Malod et al.*, 1993; *Sieh and Natawidjaja*, 2000; *Nielsen et al.*, 2004; *Curray*, 2005; *Socquet et al.*, 2006; *Raju et al.*, 2007], including topographic maps, aerial photographs, geological field observations, seismic reflection and refraction profiles, gravity data, magnetic anomalies, and GPS measurements. These data were then digitized and georeferenced, using a Geographic Information System (GIS) software.

[17] 2. For land, where these data were not available or of unsuitable quality, we reexamined SRTM digital elevation data.

[18] 3. However, these two approaches yield a nonglobal and a nonhomogeneous coverage, with both detailed small-scale maps of the faults and areas with low spatial resolution. We thus selected the major structures to avoid unnecessary detailed levels, and in this process nearby faults were grouped at some places, and at some other places the faults traces were simplified.

[19] 4. The resulting GIS document includes fault geometry and sense of fault slip from the Sunda Strait to Myanmar with a spatial resolution of ~4 km. Two zones are distinguished with different deformation styles: (1) the Sumatra zone characterized by a complex sliver plate bounded by the Sumatra and the Mentawai faults and (2) the Andaman-Burma zone characterized by a relatively simple system where only the Andaman-Sagaing Fault system is accommodating the oblique convergence of motion [e.g., *Socquet et al.*, 2006].

[20] The Sumatra fault was generalized from the map of *Sieh and Natawidjaja* [2000] and its connection with the fore arc structures from *Pertamina-Beicip* [1988]. Regional sigmoid relay zones have been taken into account and the Sumatra fault was drawn with several splays in front of We Island (in front of Aceh along strike Sumatra). The map of the fore arc basin is simplified from the DOTSEA Atlas [*Pubellier et al.*, 2005], which compiled structures mapped by *Kemal* [1993], *Malod et al.* [1993], and *Malod and Kemal* [1996], as well as local maps from *Matson and Moore* [1992] and *Beaudry and Moore* [1985]. The main tectonic element is the Mentawai fault [*Diament et al.*, 1992] which controls several morphostructural horsts and basins. These structures have been simplified as a single line passing offshore Siberut island with strike-slip and reverse components. The faults connect northward to the Nias basin hereafter regarded as a simple right-lateral transtensional area which connects via the Batee fault to the main Sumatra fault. Another simplified splay of the Mentawai fault zone runs in an E-W direction to connect to the Aceh basins and the Tuba Ridge [*Kemal*, 1993]. This segment is considered transpressional in the model up to the central part of the Tuba ridge.

[21] The Sumatra fault connects to the north to the West Andaman Fault (WAF), assumed to accommodate most of the right-lateral motion between

India-Australia and Sunda plates. The overall trace of the main WAF fault is well constrained from previous work [*Curray*, 2005], but recent marine cruises revealed a complex second-order fabric in particular at the junction with the main Central Andaman Rift where a ridge propagator is currently active [*Raju et al.*, 2004, 2007]. We included these complexities in the model to test which of these structures would be favorably triggered. The northern Andaman Rift and its transform connection with the Central Andaman Rift were mapped from the Andaman 2000 marine cruise. The surface deformation suggests that the transform fault is a series of transtensional relays rather than a through-going shear fault. Faults that connect the Andaman spreading system to the Sagaing Fault were derived from a combination of marine and land survey summarized by *Vigny et al.* [2003] and *Socquet et al.* [2006]. We further assumed that in the southern Myanmar oblique motion is partitioned between the trench and the Sagaing fault with little deformation in between [*Nielsen et al.*, 2004; *Socquet et al.*, 2006].

2.4. Friction and Skempton Coefficient

[22] Laboratory experiments typically find values for μ of around 0.6 to 0.85 for most rock material, apart from those rich in clay minerals [*Byerlee*, 1978]. The Skempton coefficient is a less well known parameter ranging between 0.4 and 0.9 for granite, sandstone and marble [*Roeloffs*, 1996], but still unconstrained for other rocks. Values of μ' between 0 and 0.75 are considered plausible [*King et al.*, 1994]. When μ' is high, the pore pressure does not strongly affect the normal stress. At the other extreme, when $\mu' = 0$, the rock is so saturated that the pore pressure annihilates the effect of the normal stress on the plane. Since μ and B are still unknown at the field scale, we try a range of values for these two parameters between 0 and 1, which allows us to test the effect of friction and fluid pressure on the failure plane.

2.5. Earthquake Catalogue

[23] In this paper we compare the calculated Coulomb stress change with the location of seismicity after the 2004 Aceh earthquake. This comparison requires a high-quality catalogue. We use the relocated earthquake catalogue obtained by *Engdahl et al.* [2007], for which the estimated accuracy in epicenter position is better than 15 km. This catalogue covers the time period between 40 years before and 2 years after the 2004 Aceh

earthquake. The area is limited to longitudes 90°E to 101°E and latitudes −3°N to 18°N.

[24] Assuming a power law distribution of earthquakes with magnitude, we estimate a minimum magnitude of completeness of 4.5. Most of the earthquakes are related with underthrusting along the megathrust fault. Since we are merely interested in stress effects on faults that are off the subduction plane, we selected shallow earthquakes (≤30 km) 120 km away from the trench with magnitude greater than 4.5. Furthermore, we use focal mechanisms from Global CMT catalogue (Harvard Seismology), which have been relocated using our modified Engdahl's catalogue. Our final earthquake catalogue consists of 495 hypocenters before the 2004 Aceh earthquake and 616 hypocenters after, for which 83 focal mechanisms are available.

3. Results

3.1. Stress Change Along the Sagaing-Andaman-Sumatra Fault System

[25] In this section we explore the impact of the Aceh and Nias earthquakes on the stress change along the Sagaing fault (SF), the Andaman rift zone, the West Andaman fault (WAF) and the Sumatra fault system (SFS). To guide the readers through our input values selection, we use the slip distributions of *Chlieh et al.* [2007] and *Briggs et al.* [2006] as the reference model (model 1). We then use the failure planes geometry described in section 2.3 and depicted on Figure 4 to calculate the $\Delta\tau$ and $\Delta\sigma_n$.

[26] We first calculate the stress change due to the 2004 Aceh earthquake alone and compare it to the earthquakes distribution that followed the next three months, i.e., just before the Nias earthquake.

[27] Shear stress change $\Delta\tau$ has a complex distribution pattern (Figure 5a). Our calculations give a $\Delta\tau < 0$ (inhibit slip) on the SF, the normal faults of the Andaman rift zone and on the right-lateral strike slip WAF in Andaman Sea. In contrast, we obtain a $\Delta\tau > 0$ on the other segments of the WAF and along the northern portion of the SFS.

[28] Normal stress change $\Delta\sigma_n$ and pressure change ΔP have a more simple pattern with a general decrease ("unclamping"), except on the Aceh back thrust and in the central part of the SFS south of the Toba lake (Figures 5b and 5c). As previously mentioned by *Brink and Lin* [2004] for
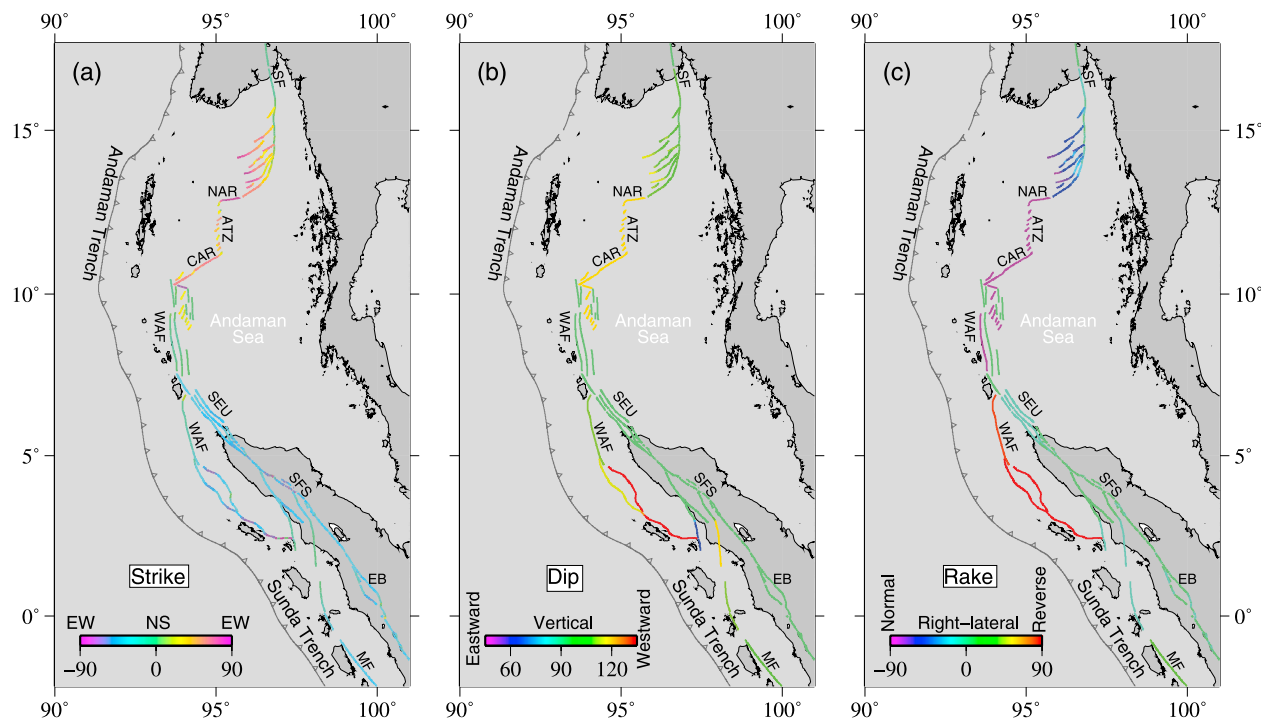
Figure 4. Geometry of the failure planes is given with strike, dip, and rake angles of faults. See Figure 1 for fault labels. (a) Strike is measured clockwise from north and is given in the two first quadrants. (b) Dip < 90° for faults dipping east. Conversely, dip > 90° for faults dipping west. (c) Rake = 0° for right-lateral strike slip fault. Rake = −90° for normal fault. Rake = 90° for reverse fault.
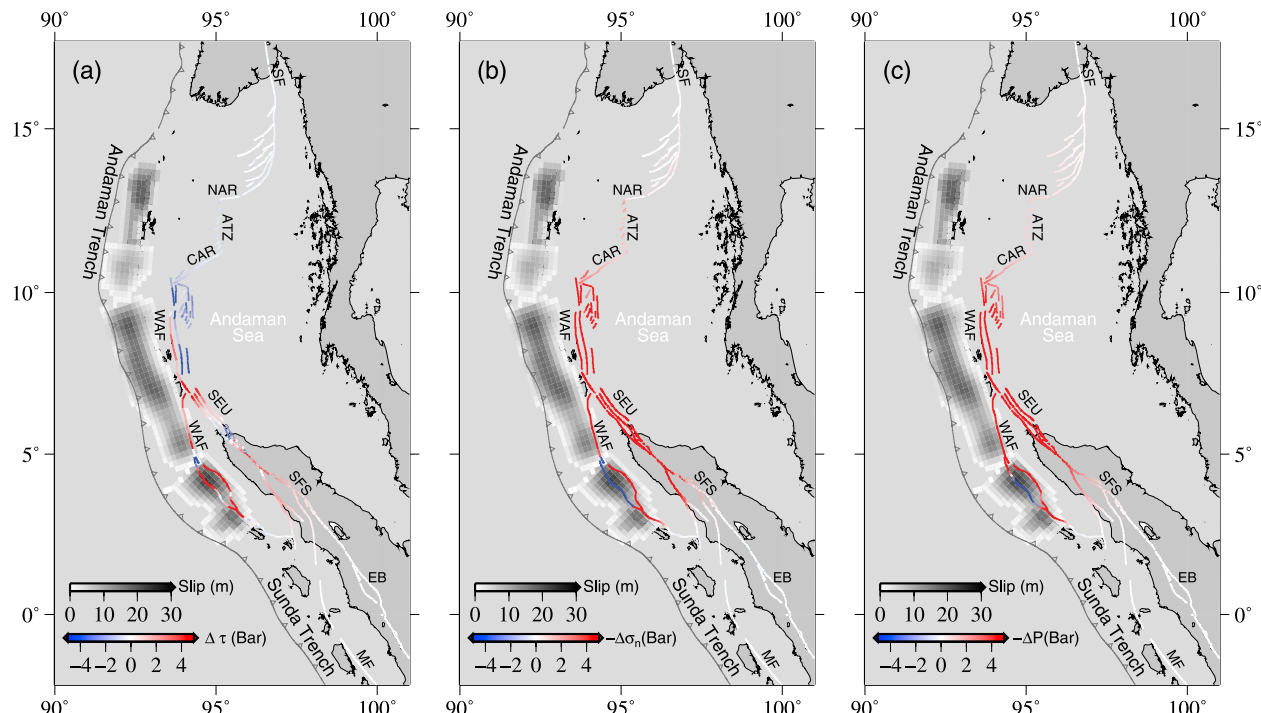
Figure 5. Stress change at 15-km-depth associated with the slip distribution proposed by *Chlieh et al.* [2007] for the 2004 Aceh earthquake. See Figure 1 for fault labels. (a) Shear stress change (positive in the direction of fault slip). (b) Normal stress change (positive if the fault is clamped). (c) Pressure change (positive in extension).
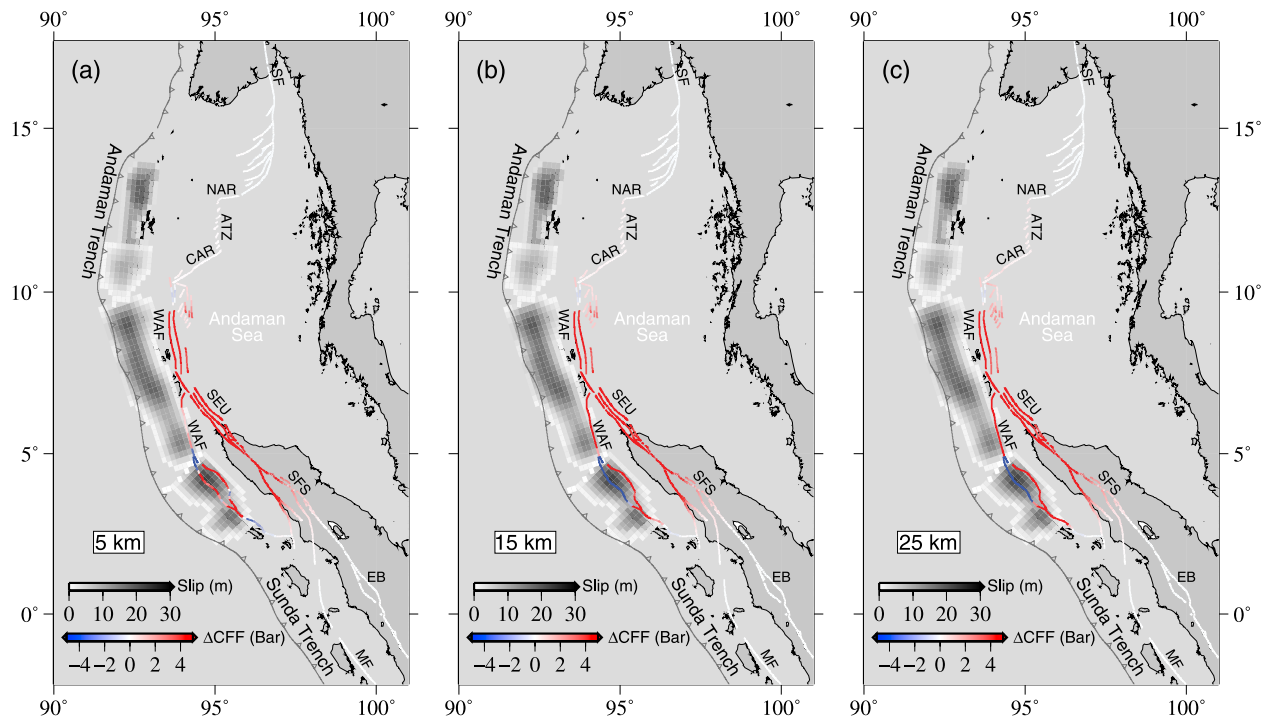
Figure 6. Variation of the calculated Coulomb stress change ΔCFF with depth. ΔCFF is positive if stress change promotes failure. Gray scale gives the slip distribution proposed by *Chlieh et al.* [2007] for the 2004 Aceh earthquake. See Figure 1 for fault labels. Associated with depths of (a) 5 km, (b) 15 km, and (c) 25 km.

the northern Caribbean plate boundary, this reduction of normal stress suggests that a significant contribution to Coulomb stress increase comes from unclamping of the faults.

[29] This preliminary analysis illustrates how the stress change due to the Aceh earthquake can inhibit or promote failure on some of the preexisting faults. Whatever the effective friction, failure is encouraged on segments with $\Delta\tau > 0$ and $\Delta\sigma_n < 0$. For the other segments, a Coulomb stress approach is required. We next assume an effective friction coefficient of 0.6 and we calculate from equation (5) the Coulomb stress change ΔCFF.

[30] The seismogenic depth reaches 30 km for some of the faults [*Engdahl et al.*, 2007], which is everywhere above the estimate of the Moho depth [*Simoes et al.*, 2004]. ΔCFF is thus calculated at a depth ranging from 5 km to 25 km. Our results suggest that depth has only a minor effect on ΔCFF (Figure 6). Thus, in the following we compare the seismicity from our modified catalogue (see section 2.5) with the distribution ΔCFF calculated for a depth of 15 km only.

[31] Following *Hardebeck et al.* [1998] we also calculate the Coulomb index *CI*, which is the percentage of earthquakes consistent with Coulomb stress change. *CI* = 50% for a random distribution

of stress change and values of *CI* between 60% and 70% are commonly obtained for the well-studied earthquakes [e.g., *Hardebeck et al.*, 1998; *Stein*, 1999; *Loevenbruck et al.*, 2004]. Here the stress changes found on the modeled faults are almost all positive, so the probability of a randomly placed earthquake in a positive zone is ∼65%, which is the percentage of the total modeled fault length with ΔCFF > 0. Compared to this value we obtain a very good agreement between the location of seismicity and the ΔCFF with a *CI* up to ∼85% (Figure 7).

[32] We first consider the time period between the Aceh and the Nias earthquakes. Major increases are on the WAF and the northern part of the SFS. This gives a simple explanation for the 2005 Andaman swarm as well the observed seismicity north of the Toba Lake (Figure 7a). Furthermore the obtained ΔCFF < 0 for the North Andaman rift as well as for the SF suggests that the 2004 event has inhibited failure, which is consistent with the low seismic activity observed along these structures during the last 40 months. The main discrepancy is in the Andaman rift zone where no earthquake has occurred three months after the event in spite of Coulomb stress increase. This discrepancy is only related to the assumed time period (before the 2005 Nias earthquake) since
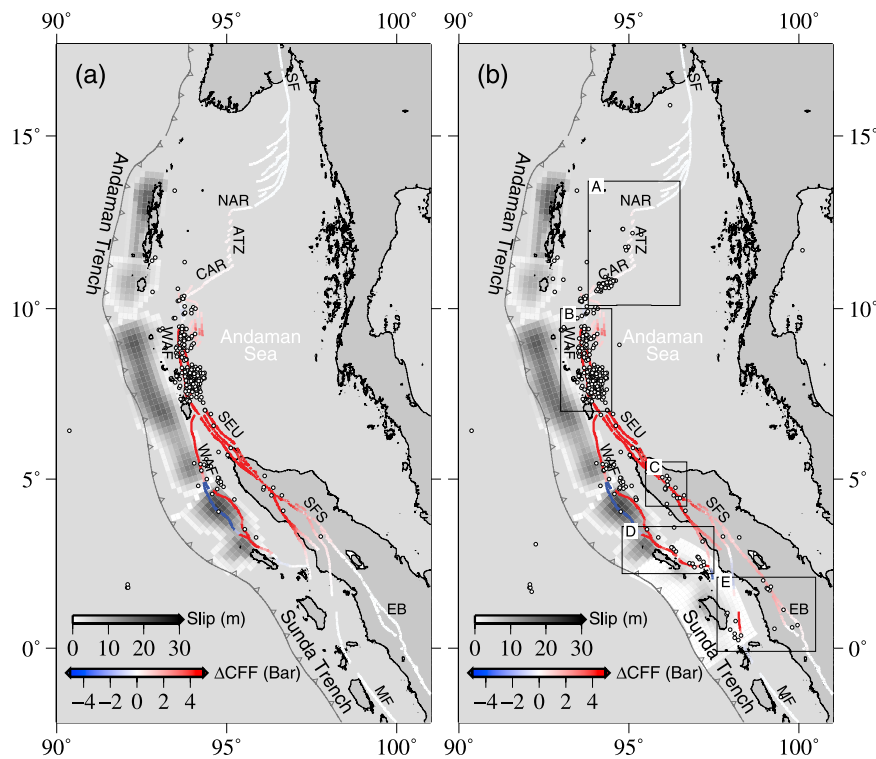
Figure 7. Calculated Coulomb stress change associated with two different time periods. White circles give the location of shallow seismicity (<30 km) corresponding to these time periods [*Engdahl et al.*, 2007]. See Figure 1 for fault labels. (a) After the 2004 Aceh earthquake and prior to the 2005 Nias earthquake. Gray scale indicates the slip distribution used in the calculation for the 2004 Aceh earthquake [*Chlieh et al.*, 2007]. (b) After both the 2004 Aceh and the 2005 Nias earthquakes. The slip distribution corresponds to the slip proposed by *Chlieh et al.* [2007] for the Aceh earthquake plus the estimated slip proposed by *Briggs et al.* [2006] for the Nias earthquake. The displayed seismicity corresponds to a time period of 2 years after the Aceh earthquake. Black boxes indicate the location of the areas presented in Figures 8–12.

intense seismic activity occurred in March 2006 along the Central rift.

[33] We then next calculate the Coulomb stress change due to the 2004 Aceh and 2005 Nias earthquakes and compare it with the seismicity covering a period of 2 years after the 2004 event. The obtained *CI* is extremely good (up to 88%). This high value is related to the occurrence of seismicity in the central Andaman rift and to the consistency between the southward propagation of seismicity and the Coulomb stress increase in central Sumatra after the Nias earthquake (Figure 7b).

3.2. Regional Studies

[34] Here we focus on areas where active seismicity has been observed since the 2004 main shock. For these small-scale regional studies the assumptions used in assigning one given earthquake to one particular faults are not obvious. As previously mentioned the estimated accuracy of epicenter position is ∼15 km. We estimate that our GIS

database for fault geometry and sense of fault slip has a spatial resolution of ∼4 km which results from the faults selection process. Thus our approach cannot be used to explain neither the location of seismicity far from the main structures nor the diversity of aftershock mechanisms that occur in close proximity. However many of the recorded earthquakes are quite close to the major structures that we selected. Focal mechanisms, where available, indicate in most cases one focal plane in line with the local trend of the faults. We thus feel rather confident that the earthquakes that occurred onto the Sumatra fault and tributaries as well as within the rift segments of the Andaman basin are representative of the mapped fault (mainly right-lateral strike-slip and normal faults). However, at some other places (offshore Sumatra), we cannot rule out that some of the earthquakes actually occurred on satellite planes, such as conjugate planes. Some regions may also be affected by a complex style of deformation with compatible but mixed mechanisms. Although we do acknowl-
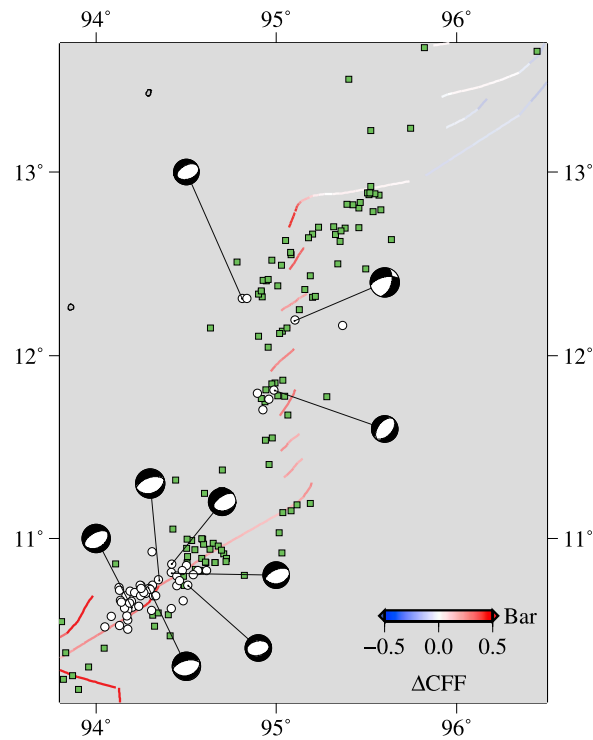
Figure 8. Calculated Coulomb stress due to both the 2004 Aceh and the 2005 Nias earthquakes in the Andaman rift zone (see location box A on Figure 7). Green squares give indicate the seismicity of the 40 years prior to the 2004 Aceh earthquake [*Engdahl et al.*, 2007]. White circles indicate the 2 years of seismicity posterior to the 2004 Aceh earthquake [*Engdahl et al.*, 2007]. Focal mechanisms after the Aceh earthquake from CMT catalogue (Harvard Seismology) are plotted at the location of relocated seismicity. Note the change in the range of the color scale.

edge that this may affect our calculations, our option was to choose the geometry and style of the nearest major structure which is not more ad hoc than using the optimally oriented planes.

3.2.1. Andaman Rift Zone

[35] The earthquakes are consistent with normal-faulting mechanisms oriented perpendicular or near perpendicular to the structures. This strengthens our assumptions on geometry and rake, in particular for the deeper part of the Andaman transform zone which forms a large-scale en echelon system. A swarm of earthquake affected the Central rift between 9 and 11 March 2006, with magnitude not exceeding 5.5. The calculated Coulomb stress increase at this location is ∼0.3 bar, which is a very low perturbation (Figures 7 (box A) and 8). To investigate this issue we examined carefully the available seismicity recorded over the last 40 years. We found that similar swarms actually

affected the Andaman Basin faults before, in 1983–1984 [*Guzmán-Speziale and Ni*, 1993], in 1993 and just before the great December earthquake in the summer 2004. The March 2006 swarm broke a segment of the Central rift that had not been broken at least in the last 40 years. Altogether, the three swarms broke a significant length of the Central Andaman rift. As proposed elsewhere [e.g., *Stein*, 1999; *Pollitz et al.*, 2006], this underlines the primary effect of the state of stress on the failure occurrences and the need for a good knowledge of the seismic history of the region.

3.2.2. Swarm and Normal Faulting Along the West Andaman Fault

[36] The Andaman Sea basin north of Sumatra has been one of the most active areas after the 2004 earthquake [*Lay et al.*, 2005]. This intense activity involved more than 270 earthquakes with magnitude between 4.5 and 5.8 that occurred from 26 to 31 January 2005. By definition these events are secondary aftershocks which have been triggered not only by the Aceh stress field, but also by the stress changes induced by the aftershocks themselves. This secondary triggering is beyond the scope of this study, so we do not discuss the size of this swarm and its time evolution. We rather focus on the stress field related to the Aceh event and the seismicity prior to the occurrence of this swarm.

[37] First our results give a ΔCFF of ∼3 bar, which promotes failure in the region of the West Andaman fault for normal as well as right-lateral faulting (Figures 7 (box B) and 9). Furthermore the analysis of seismicity prior to the 2004 event reveals that (1) few moderate earthquakes (M ≥ 4.5) occurred in this area during the last 40 years and (2) previous swarms events have occurred south (e.g., March–April 1976, January 1982) and north (e.g., July 1976, October 1994) of this region. Altogether, these observations suggest that although the 2005 swarm occurrence was most probably triggered by the Aceh earthquake, the swarm location itself relates to stress transfer along the WAF.

[38] As previously noticed by *Engdahl et al.* [2007], most of the events that occurred north of this swarm after the 2004 earthquake are characterized by normal-faulting mechanisms, whereas prior to 2004 most of the seismicity was consistently right-lateral strike-slip. To investigate this issue, stress change was calculated using two different rake angles 0° and −90° for the WAF
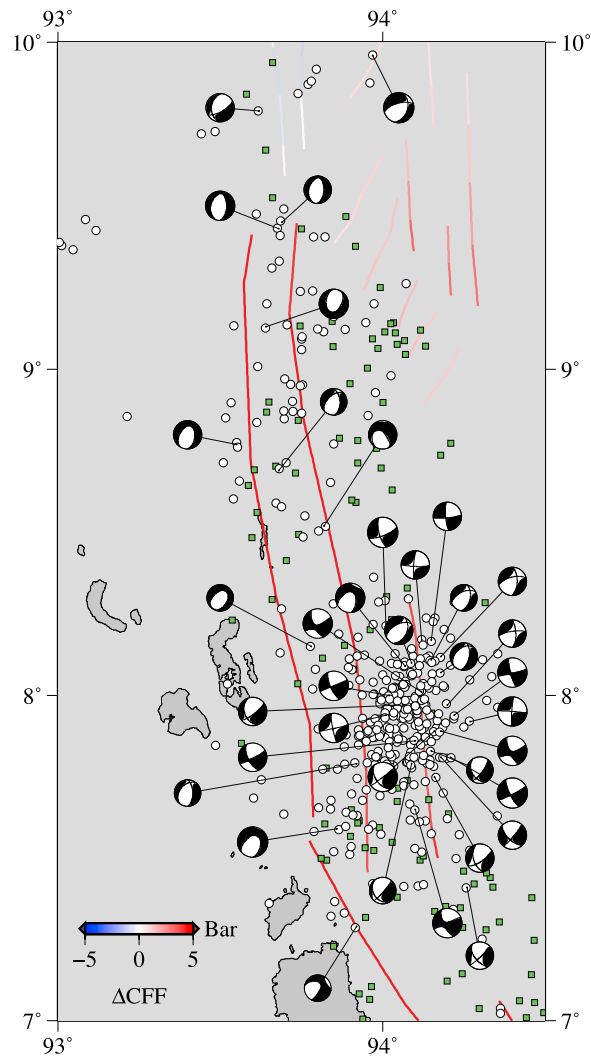
Figure 9. Same as Figure 8 for the region of the West Andaman Fault (see location box B on Figure 7).

(see Figure 4). Whatever the assumed rake, our results give a Coulomb stress increase (Figure 9). The detailed analysis of shear and normal stress suggests, however, that only normal faulting favors a shear stress increase on the WAF (Figure 5). We thus propose to interpret the variations in time of focal mechanisms as the result of stress change. Prior to the 2004 earthquake, the state of stress along the WAF was mainly driven by interseismic motion, which favors right-lateral strike slip. In contrast after 2004, the main shock impacts significantly the state of stress, which temporarily favors normal-faulting events.

3.2.3. Northern Sumatra

[39] Our calculations give a maximum for the Coulomb stress increase in the northern part of the SFS (Figures 7 (box C) and 10). This result is in

agreement with previous studies [e.g., *McCloskey et al.*, 2005] and is consistent with both the location of seismicity and the focal mechanisms after the 2004 and 2005 events. In this region the Coulomb stress increase reaches 20 bar. This high value and the lack of major earthquake at least in the last 170 years [*Bellier et al.*, 1997; *Sieh and Natawidjaja*, 2000] along this ~200-km-long segment result in a high seismic hazard for this region.

3.2.4. Simeulue Area

[40] The Simeulue Island marks the southern and northern termination of the 2004 and 2005 earthquakes, respectively. This is a key region to study the southward propagation of ΔCFF due to these two events (Figures 7a and 7b). The location of seismicity is in good agreement with the calculated ΔCFF for both earthquakes (Figures 7a and 7b). However, the CMT solutions give normal- and reverse-faulting mechanisms oriented perpendicular or near-perpendicular to the offshore thrust fault (Figures 7 (box D) and 11). This cannot be easily interpreted in terms of geometry and would require a detailed study of tectonic features as well as a reassessment of focal mechanisms in this region, which are out of the scope of the present paper.

3.2.5. Batee-Mentawai Fault and Central Sumatra

[41] This region marks the southern limit of both $\Delta CFF > 0$ and earthquakes occurrence. Along the
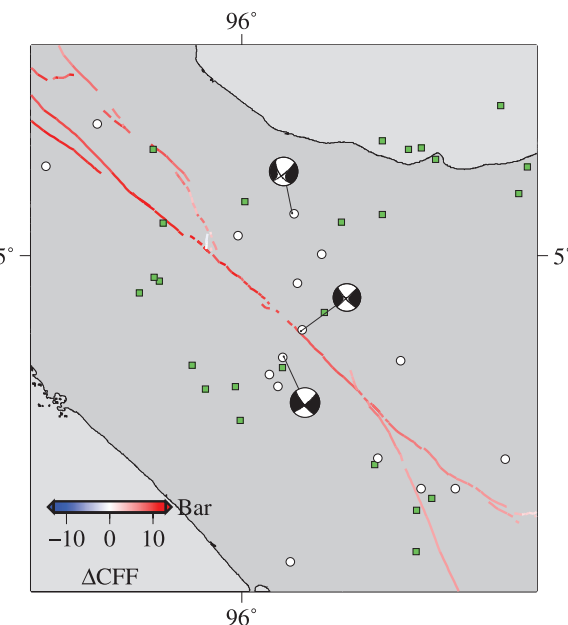

Figure 10. Same as Figure 8 for the northern part of the Sumatra Fault System (see location box C on Figure 7).
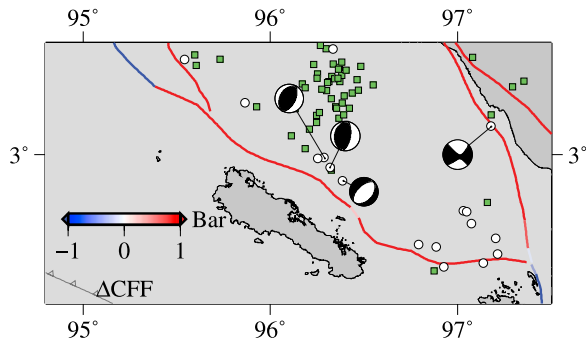
Figure 11. Same as Figure 8 for the Aceh back thrust (see location box D on Figure 7).

Batee-Mentawai fault system our results are in good agreement with both the location of seismicity and right-lateral strike-slip mechanisms (Figures 7 (box E) and 12). In particular, note that most of the seismicity is located above the rupture of the 2005 rupture where $\Delta CFF > 0$.

[42] Along the SFS most of the events prior to and after 2004 are located at 1.8°N. This may be related to Coulomb stress increase and to the particular geometry of the Sumatra fault in this area, which splits into two branches: the Barumum segment and the Angkola segment bounding the Equatorial Bifurcation [*Sieh and Natawidjaja*, 2000]. $\Delta CFF > 0$ along these two branches, except on the southernmost part of the Angkola segment (Figure 12). This result seems to be in disagreement with the location of the magnitude 5.8 earthquake, which occurred in December 2006 near this last segment. However, the associated strike-slip focal mechanism is not consistent with the orientation of this segment. This suggests that the rupture did not occur along this segment but rather along either the Barumum segment or the northern Angkola segment, which requires an error of ∼20 km in epicenter location.

4. Sensitivity to the Coseismic Slip Distribution

[43] In the previous part ΔCFF has been calculated from the slip distribution obtained by *Chlieh et al.* [2007] and by *Briggs et al.* [2006] for the 2004 Aceh and the 2005 Nias earthquakes, respectively. However we have shown in section 2.2 that many models have been proposed for these two events. Here we compare ΔCFF predicted by nine models, which combine the models proposed by *Chlieh et al.* [2007], *Rhie et al.* [2007], and *Fujii and Satake* [2007] for the 2004 event with the models obtained

by *Briggs et al.* [2006], *Banerjee et al.* [2007], and C. Ji (Preliminary result of the Mar 28, 2005 Mw 8.68 Nias Earthquake, 2005, available at http://www.geol.ucsb.edu/faculty/ji/big_earthquakes/home.html) for the 2005 event (see Table 1).

[44] Altogether the tested models show common features with Coulomb stress increase between 0° and 10°N along the central and the northern part of the Sumatra fault system as well as along the West Andaman fault (Figure 13). Yet, differences can be noticed. First, models 7–9 related to *Fujii and Satake*'s [2007] model give extremely low ΔCFF (<0.02 bar) in the Andaman rift zone, which is not consistent with the seismic activity observed within the Central Andaman Rift and along the Andaman Transform Zone. This suggests a northward propagation of the 2004 rupture at least to the latitude of the Andaman Island, which is consistent with the location of aftershocks along the Sunda-Andaman megathrust as well as GPS measurements in Myanmar [*Vigny et al.*, 2005]. Second, models 7–9 also predict $\Delta CFF < 0$ along the offshore thrust fault between Simeulue and Banyak Islands, which is not consistent with the seismic activity observed at this location. This suggests that a slip of 20 m at the southern end of *Fujii and Satake*'s [2007] model is overestimated and that a lower slip of 0–10 m as proposed by *Chlieh et al.* [2007] and *Rhie et al.* [2007] is more realistic.

[45] The differences between models 1–6 are mostly related to the magnitude of ΔCFF rather than to its general pattern. Only slight differences between the two models of Aceh earthquake can be observed, except along the northern WAF and the offshore thrust north of Simeulue Island, for which
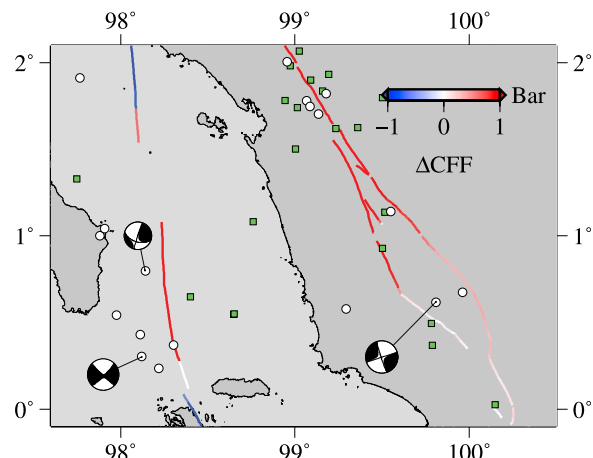

Figure 12. Same as Figure 8 for the central Sumatra Fault System and the northern part of the Mentawai Fault (see location box E on Figure 7).
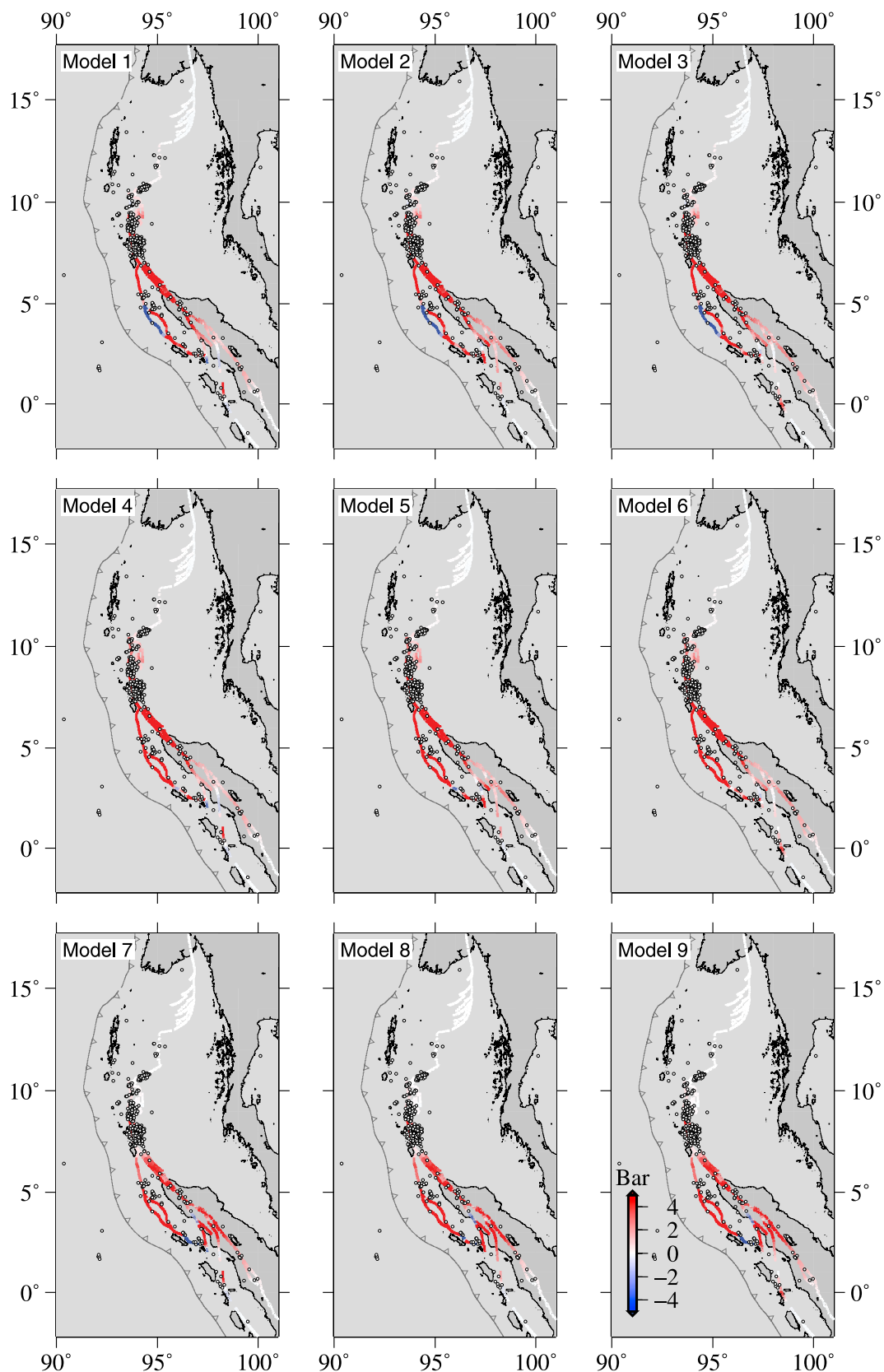
Figure 13. Effect of the assumed coseismic slip distribution on the calculated Coulomb stress change (see Table 1 for references).
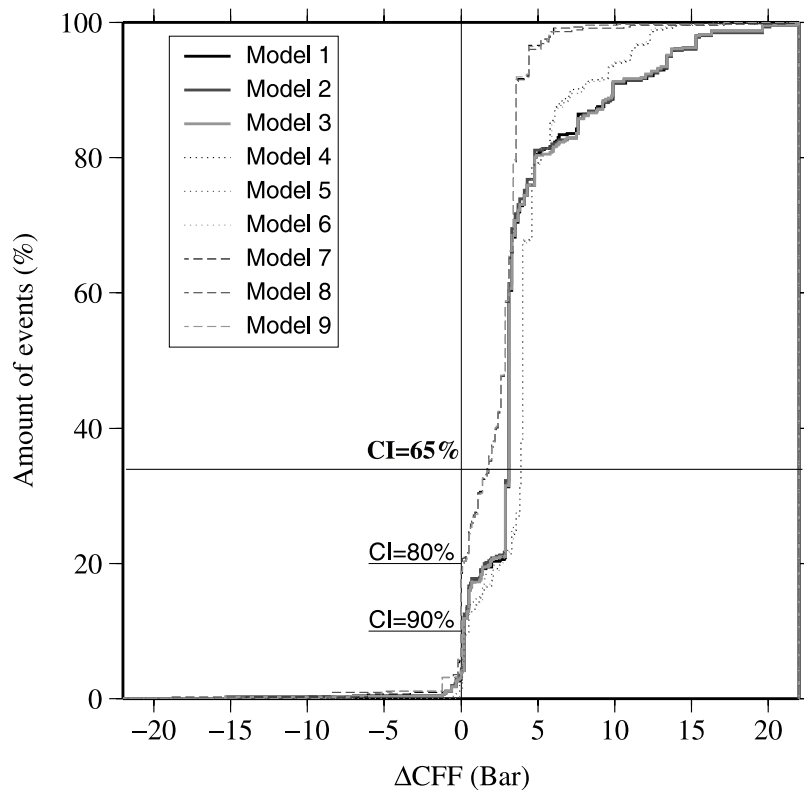
Figure 14. Relationship between the amount of Coulomb stress change and the occurrence of events for the tested slip distributions (see Table 1). *CI* is the Coulomb index.

Rhie et al.'s [2007] model gives an increase in Coulomb stress. In the same way, the assumed model for the Nias earthquake has only a minor effect on ΔCFF and the differences cannot be tested with the available seismicity.

[46] To further compare these models, we assigned to each aftershock the value of the closest calculated ΔCFF. The assumed model has a minor effect on the *CI*, which ranges between 80% and 90%. The role of the Coulomb stress change in controlling earthquakes occurrence is illustrated in Figure 14, where we plot for each model the number of events as a function of ΔCFF. Our results indicate that (1) the trends of models 7−9 differ from those of model 1−6, (2) models 1−6 show only minor differences, (3) only 10−20% of the total events are associated with a low Coulomb stress increase (<2 bar), and (4) 50% are due to an increase of ∼3 bar, which is related to the great Andaman swarm.

[47] This comparison confirms that the use of models 1−6 is relevant to calculate the ΔCFF associated to the Aceh and the Nias earthquakes,

and thus strengthens the previous results obtained using model 1.

5. Influence of Fault Friction

[48] The calculation of ΔCFF requires information on both friction coefficient and pore pressure (see equation (3)). Although the parameters μ and B are seldom assessed at field scale, a value of 0.4 for the effective friction coefficient is commonly used [e.g., *King et al.*, 1994; *Pollitz et al.*, 2006]. We use here model 1 to test the robustness of our results for μ and B between 0 and 1.

[49] The distribution of the Coulomb index suggests that the friction coefficient has a primary effect on the agreement between seismicity and ΔCFF (Figure 15). Our approach is relevant (*CI* > 65%) only for μ > 0.6, which is consistent with the values estimated from laboratory experiments on rocks. In this range of μ, a wide range of B can properly explain the aftershocks location, but a decrease in B significantly improves the *CI*. Figure 15 shows contours of equal effective friction assuming that $B = B'$ in equation (5). Note that
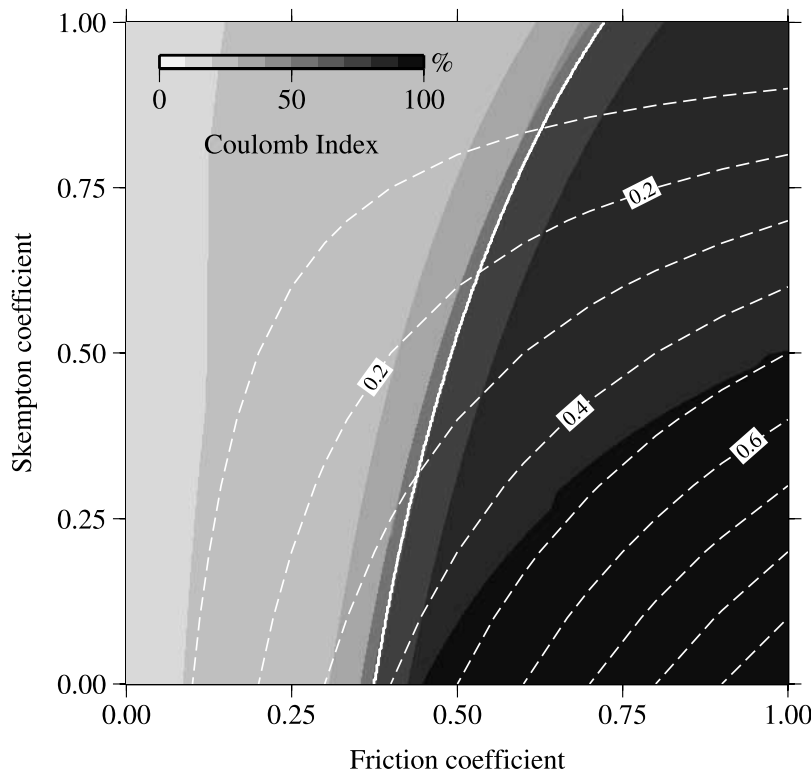
Figure 15. Effect of the friction and the Skempton's coefficients on the obtained Coulomb index. The assumed slip distribution corresponds to model 1 [*Chlieh et al.*, 2007; *Briggs et al.*, 2006]. Solid white line corresponds to a Coulomb index of 65%. Dashed lines give the value of the effective friction coefficient assuming that $B = B'$ in equation (5).

these curves are parallel to the Coulomb index distribution only for high effective friction ($\mu' > 0.45$). As previously mentioned by *Cocco and Rice* [2002], this suggests that the ratio B'/B is not constant. Thus, the effective friction coefficient μ' is not a material property, but a parameter depending on the ratio of stress change in the medium.

[50] As previously mentioned, if $\Delta\tau > 0$ and $\Delta\sigma_n < 0$ then $\Delta CFF > 0$ whatever the assumed effective friction. Here we calculate the distribution of ΔCFF using μ' between 0 and 1. In contrast with *Nalbant et al.* [2005], our results depend on the value of μ' (Figure 16). For instance, because of the ratio between $\Delta\tau$ and $\Delta\sigma_n$ the seismicity in the Andaman rift zone can only be explained if $\mu' > 0.5$. On the basis of this result, we assess the spatial distribution of the lower bound on μ' along major faults with aftershocks activity (Figure 17).

[51] Our study gives no constraints on friction (e.g., $\mu' > 0-0.1$) along the major thrust and strike-slip faults, which include the SFS, the offshore thrust faults and the WAF. In contrast, only moderate to high effective friction coefficients ($\mu' > 0.4-0.5$) can explain seismic activity along the central Andaman rift and the Andaman trans-

form zone, which is consistent with friction inferred for high-angle normal faults [see *Collettini and Sibson*, 2001, and references therein]. This spatial variation of the lower bound on μ' may be regarded as an artefact related to the nonhomogeneous distribution of GPS observations, which leads to a better resolution of the slip distribution along the western coast of Sumatra Island. However, our sensitivity tests to coseismic slip distribution indicate a similar pattern for models 1 to 6, with a clear ΔCFF variation between the WAF and the Andaman rift zone, which can be related to shear stress decrease along the central Andaman rift. This confirms that the obtained spatial variation of the lower bound on μ' is robust to large ranges of slip models.

[52] On the basis of these results two end-member models can be proposed. A first model is to assume a constant effective fault friction. In this case a high coefficient of friction (>0.6) is required to explain the observations. This value is in agreement with the measurements of laboratory friction, but it is not consistent with low friction coefficient (<0.2) estimate at field scale for other subduction zones [e.g., *Cattin et al.*, 1997; *Buiter et al.*, 2001] as well
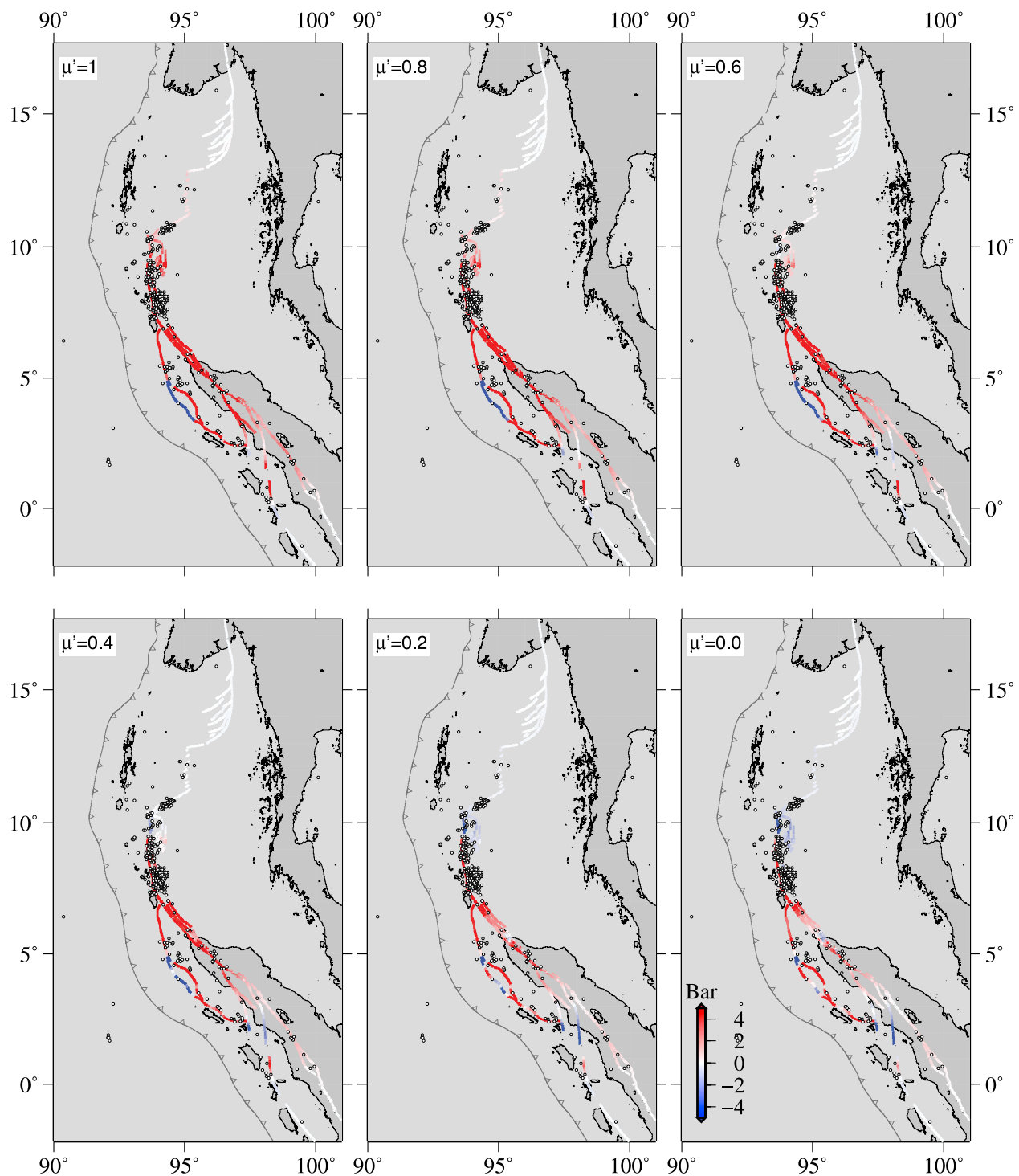
Figure 16. Effect of the effective friction coefficient on the calculated Coulomb stress change assuming the model 1 for the coseismic slip distribution [*Chlieh et al.*, 2007; *Briggs et al.*, 2006].

as along major strike-slip faults [e.g., *Provost et al.*, 2003; *Townend and Zoback*, 2004; *Vernant and Chéry*, 2006]. An alternative model is that fault friction varies from fault to fault. A possible explanation is that the friction is related to the amounts of slip, as proposed by *Liu and Bird* [2002]. An other explanation is that fault friction depends on either the nature of the lithosphere, oceanic versus continental, or the fault type, thrust and strike-slip faults could be weak whereas nor-
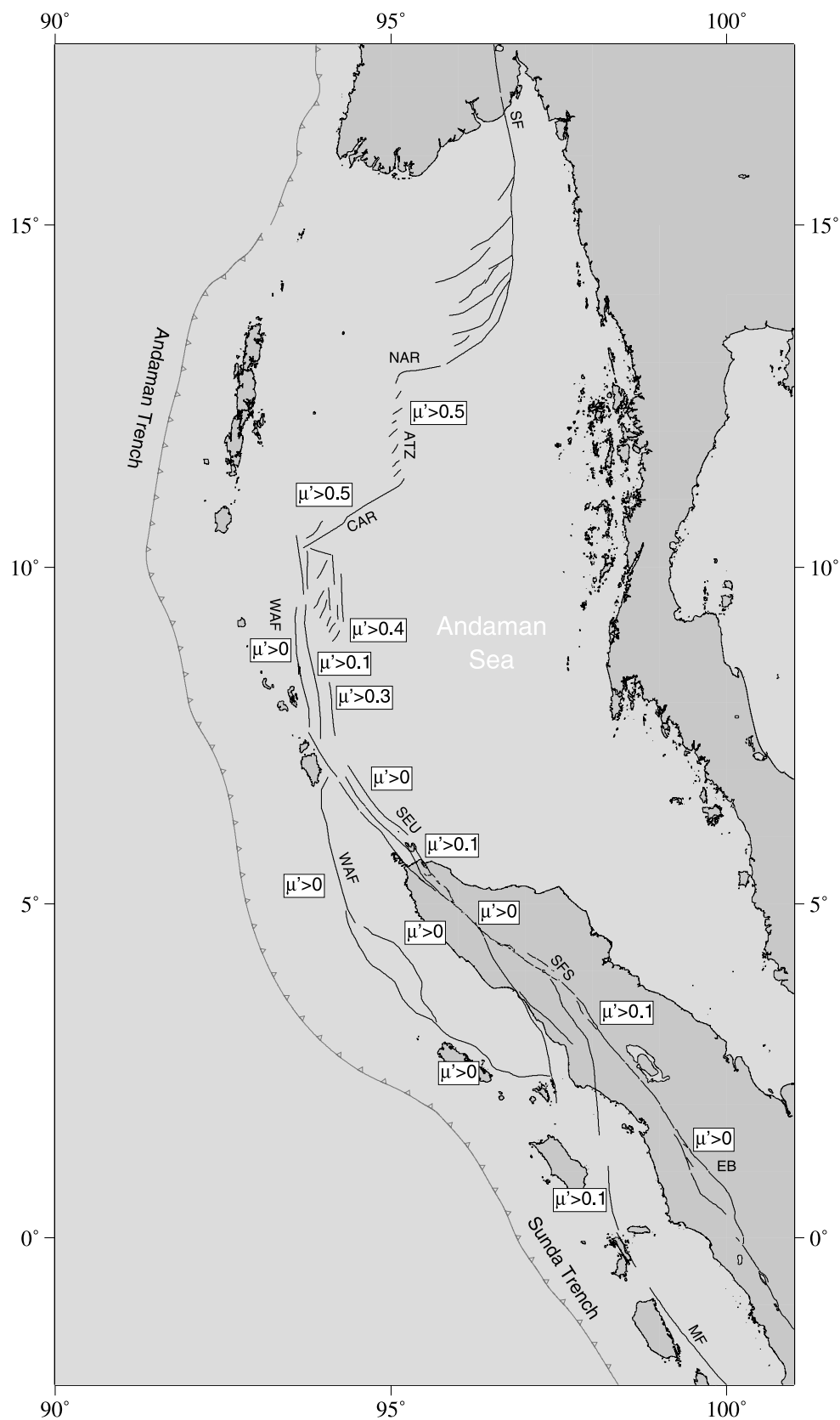
Figure 17. Estimated effective friction along the major faults in the Sumatra-Andaman region from seismicity and Coulomb stress change associated to the coseismic slip distribution of the 2004 Aceh and 2005 Nias earthquake. See Figure 1 for fault labels.

mal faults could be stronger. Yet, systematic studies of fault friction elsewhere are now needed to confirm these assumptions and to test these two models.

6. Conclusion

[53] Using both detailed mapping of failure planes and well-constrained slip distributions, we have calculated stress change associated with the 2004 Aceh and 2005 Nias earthquakes. Our results support a clear relationship between aftershocks locations and $\Delta CFF > 0$, in particular for the swarm activity in the central Andaman rift and along the WAF. We further interpret the temporal variations of focal mechanisms observed along the WAF between 8.2°N and 9.5°N as the result of stress change: prior to the 2004 earthquake, the state of stress along the West Andaman fault is mainly driven by interseismic motion, which favors right-lateral strike slip. In contrast, after 2004, the main shock significantly impacted the state of stress and temporarily favors normal-faulting events.

[54] The calculated ΔCFF suggests that the 2004 and 2005 earthquakes inhibited failure on the North Andaman rift and on the Sagaing fault, while failure was encouraged along the Andaman transform zone, the central Andaman rift, the WAF, the SFS and the offshore thrust fault west of Sumatra Island. However, as pointed out by *Stein* [1999], ΔCFF is only related to a time change in the failure occurrence. Seismic hazard assessment also requires a good knowledge of faults state of stress, which can be partly estimated from seismic history. For instance, the maximum value of $\sim 15-20$ bar for ΔCFF is reached in the northern part of the SFS. Knowing that no major earthquake have occurred at least in the last 170 years along this segment, this high ΔCFF results in a high seismic hazard for this region.

[55] The static Coulomb stress change and the observed seismic activity are in very good agreement with a Coulomb index up to $\sim 85\%$. Compared to previous studies this high Coulomb Index confirms two important issues on the use of static stress change. First, in this study we only consider far-field aftershocks. Because of Coulomb stress decrease on the rupture itself, CI will be significantly affected by considering near-field interplate aftershocks. Second, we only analyze aftershocks on large and mature faults at a time scale of several months, which is consistent with the results of the

unified model for dynamic and static stress triggering proposed by *Voisin et al.* [2004].

[56] Comparison of the ΔCFF distribution for a range of μ' between 0 and 1 reveals significant differences with important fault friction implications, leading to two end-member models: (1) a model with constant but high (>0.6) fault friction and (2) a model with spatial variation of μ', which can be related either to the nature of the crust, to the geologic history of the major faults or to the fault type.

Acknowledgments

References

Arnadottir, T., and P. Segall (1994), The 1989 Loma Prieta earthquake imaged from inversion of gedetic data, *J. Geophys. Res.*, *99*, 21,835–21,855.

Banerjee, P., F. Pollitz, B. Nagarajan, and R. Bürgmann (2007), Coseismic slip distribtions of the 26 December 2004 Sumatra-Andaman and 28 March 2005 Nias earthquakes from GPS static offsets, *Bull. Seismol. Soc. Am.*, *97*(1A), S86–S102, doi:10.1785/0120050609.

Beaudry, D., and G. Moore (1985), Seismic stratigraphy and Cenozoic evolution of West Sumatra forearc basin, *Am. Assoc. Petrol. Geol. Bull.*, *69*(5), 742–759.

Bellier, O., M. Sébrier, S. Pramumijoyo, T. Beauduin, H. Harjono, I. Bahar, and O. Forni (1997), Paleoseismicity and seismic hazard along the great Sumatran fault (Indonesia), *J. Geodyn.*, *24*(1–4), 169–183.

Briggs, R., et al. (2006), Deformation and slip along the Sunda megathrust in the great 2005 Nias-Simeulue earthquake, *Science*, *311*(5769), 1897–1901.

Brink, U., and J. Lin (2004), Stress interaction between subduction earthquakes and forearc strike-slip faults: Modelling and application to the northern Caribbean plate boundary, *J. Geophys. Res.*, *109*, B12310, doi:10.1029/2004JB003031.

Buiter, S., R. Govers, and M. Wortel (2001), A modelling study of vertical surface displacements at convergent plate margins, *Geophys. J. Int.*, *147*, 415–427.

Byerlee, J. (1978), Friction of rocks, *Pure Appl. Geophys.*, *116*, 615–626.

Cattin, R., H. Lyon-Caen, and J. Chéry (1997), Quantification of interplate couplking in subduction zones and forearc topography, *Geophys. Res. Lett.*, *24*, 1563–1566.

Chlieh, M., et al. (2007), Coseismic slip and afterslip of the great Mw 9.15 Sumatra-Andaman earthquake of 2004, *Bull. Seismol. Soc. Am.*, *97*(1A), S152–S173, doi:10.1785/0120050631.

Cocco, M., and J. Rice (2002), Pore pressure and poroelasticity effects in Coulomb stress analysis of earthquake interactions, *J. Geophys. Res.*, *107*(B2), 2030, doi:10.1029/2000JB000138.

Collettini, C., and R. Sibson (2001), Normal faults, normal friction?, *Geology*, *29*(10), 927–930.

Curray, J. (2005), Tectonics and history of the Andaman Sea region, *J. Asian Earth Sci.*, *25*, 187–228.

Das, S., and C. Scholz (1981), Off-fault aftershocks clusters caused by shear stress increase?, *Bull. Seismol. Soc. Am.*, *71*, 1669–1675.

Delescluse, M., and N. Chamot-Rooke (2007), Instantaneous deformation and kinematics of the India-Australia plate, *Geophys. J. Int.*, *162*(2), 818–842, doi:10.1111/j.1365-246X.2006.03181.x.

Diament, M., H. Harjono, K. Karta, C. Deplus, D. Dahrin, M. Zen, M. Gérard, O. Lassal, A. Martin, and J. Malod (1992), Mentawai fault zone off sumatra: A new key to the geodynamics of western Indonesia, *Geology*, *20*, 259–262.

Engdahl, E., R. van der Hilst, and R. Buland (1998), Global teleseismic relocation with impoved travel times and procedures for depth determination, *Bull. Seismol. Soc. Am.*, *88*, 722–743.

Engdahl, E., A. Villaseñor, H. DeShon, and C. Thurber (2007), Teleseismic relocation and assessment of seismicity (1918–2005) in the region of the 2004 Mw 9 Sumatra-Andaman and 2005 Mw 8.6 Nias Island great earthquakes, *Bull. Seismol. Soc. Am.*, *97*(1A), S43–S61, doi:10.1785/0120050614.

Fujii, Y., and K. Satake (2007), Tsunami source of the 2004 Sumatra-Andaman earthquake inferred from tide gauge and satellite data, *Bull. Seismol. Soc. Am.*, *97*(1A), S192–S207, doi:10.1785/0120050613.

Gahalaut, V. (2005), 28 March 2005 Sumatra earthquake: Expected, triggered or aftershock?, *Curr. Sci.*, *89*(3), 452–454.

Guzmán-Speziale, M., and J. Ni (1993), The opening of the Andaman Sea: Where is the short-term displacement being taken up?, *Geophys. Res. Lett.*, *20*(24), 2949–2952.

Hardebeck, J., J. Nazareth, and E. Hauksson (1998), The static stress change triggering model: Constraints from two southern California aftershock sequences, *J. Geophys. Res.*, *103*, 24,427–24,437.

Harris, R. (1998), Introduction to special section: Stress triggers, stress shadows, and implications for seismic hazard, *J. Geophys. Res.*, *103*, 24,347–24,358.

Hill, D. (1993), Seismicity remotely triggered by the magnitude 7.3 Landers, California, earthquake, *Science*, *260*, 1617–1623.

Kemal, B. (1993), La marge active au Nord Ouest de Sumatra. Mécanismes géodynamiques de transfert liés à la subduction oblique, Ph.D. thesis, Univ. Pierre et Marie Curie, Paris.

King, G., R. Stein, and J. Lin (1994), Static stress changes and the triggering of earthquake, *Bull. Seismol. Soc. Am.*, *84*, 935–953.

Lay, T., et al. (2005), The Great Sumatra-Andaman earthquake of 26 December 2004, *Science*, *308*, 1127–1133.

Liu, Z., and P. Bird (2002), Finite element modeling of neotectonics in New Zealand, *J. Geophys. Res.*, *107*(B12), 2328, doi:10.1029/2001JB001075.

Loevenbruck, A., R. Cattin, X. L. Pichon, S. Dominguez, and R. Michel (2004), Coseismic slip resolution and post-seismic relaxation time of the 1999 Chi-Chi, Taiwan earthquake as constrained by geological observations, geodetic measurements and seismicity, *Geophys. J. Int.*, *158*, 310–326.

Ma, K., C. Chan, and R. Stein (2005), Response of seismicity to Coulomb stress triggers and shadows of the 1999 Mw = 7.6 Chi-Chi, Taiwan earthquake, *J. Geophys. Res.*, *110*, B05S19, doi:10.1029/2004JB003389.

Malod, J., and B. Kemal (1996), The Sumatra margin: Oblique subduction and lateral displacement of the accretionary prism, *Geol. Soc. Spec. Publ.*, *106*, 19–28.

Malod, J., et al. (1993), Déformation du bassin d'avant-arc au Nord-Ouest de Sumatra: Une réponse à la subduction oblique, *C. R. Acad. Sci. Paris*, *316*(II), 791–797.

Matson, R., and G. Moore (1992), Structural controls on forearc basin subsidence in the central Sumatra forearc basin, in *Geology and Geophysics of Continental Margins, AAPG Mem.*, *53*, 157–181.

McCloskey, J., S. S. Nalbant, S. Steacy, C. Nostro, O. Scotti, and D. Baumont (2003), Structural constraints on the spatial distribution of aftershocks, *Geophys. Res. Lett.*, *30*(12), 1610, doi:10.1029/2003GL017225.

McCloskey, J., S. Nalbant, and S. Steacy (2005), Earthquake risk from co-seismic stress, *Nature*, *434*, 291.

Mignan, A., G. King, D. Bowman, R. Lacassin, and R. Dmowska (2006), Seismic activity in the Sumatra-Java region prior to the December 26, 2004 (M_w = 9.0–9.3) and March 28, 2005 (M_w = 8.7) earthquakes, *Earth Planet. Sci. Lett.*, *244*, 639–654, doi:10.1016/j.epsl.2006.01.058.

Nalbant, S., S. Steacy, K. Sieh, D. Natawidjaja, and J. McCloskey (2005), Earthquake risk on the Sunda trench, *Nature*, *435*, 756–757.

Nielsen, C., N. Chamot-Rooke, and C. Rangin (2004), From partial to full strain partitioning along the Indo-Burmese hyper-oblique subduction, *Mar. Geol.*, *209*(1–4), 303–327.

Okada, Y. (1992), Internal deformation due to shear and tensile faults in a half space, *Bull. Seismol. Soc. Am.*, *82*, 1018–1040.

Omori, F. (1894), On the aftershocks of earthquake, *Tokyo Imp. Coll. Sci.*, *7*, 111–200.

Pertamina-Beicip (1988), Geological map of western Indonesia, scale 1:2.000.000, Jakarta.

Pollitz, F., P. Banerjee, R. Bürgmann, M. Hashimoto, and N. Choosakul (2006), Stress change along the Sunda trench following the 26 December 2004 Sumatra-Andaman and 28 March 2005 Nias earthquakes, *Geophys. Res. Lett.*, *33*, L06309, doi:10.1029/2005GL024558.

Provost, A., J. Chéry, and R. Hassani (2003), 3D mechanical modelling of the GPS velocity field along the North Anatolian fault, *Earth Planet. Sci. Lett.*, *209*, 361–377.

Pubellier, M., C. Rangin and F. Ego, et al. (2005), Atlas of the margins of SE Asia, *Map 176*, Geol. Soc. of Fr., Paris.

Raju, K. A. K., T. Ramprasad, P. S. Rao, B. R. Rao, and J. Varghese (2004), New insights into the tectonic evolution of the Andaman basin, northeast Indian Ocean, *Earth Planet. Sci. Lett.*, *221*(1–4), 145–162, doi:10.1016/S0012-821X(04)00075-5.

Raju, K. A. K., G. P. S. Murty, D. Amarnath, and M. L. M. Kumar (2007), The west Andaman fault and its influence on the aftershock pattern of the recent megathrust earthquakes in the Andaman-Sumatra region, *Geophys. Res. Lett.*, *34*, L03305, doi:10.1029/2006GL028730.

Rhie, J., D. Dreger, R. Bürgmann, and B. Romanowicz (2007), Slip of the 2004 Sumatra-Andaman earthquake from joint inversion of long-period global seismic waveforms and GPS static offsets, *Bull. Seismol. Soc. Am.*, *97*(1A), S115–S127, doi:10.1785/0120050620.

Rice, J., and M. Cleary (1976), Some basic stress diffusion solution for fluid-saturated elastic porous media with compressible constituents, *Rev. Geophys.*, *14*, 227–241.

Roeloffs, E. (1996), Poroelastic techniques in the study of earthquake-related hydrologic phenomena, *Adv. Geophys.*, *37*, 135–195.

Sagiya, T., and W. Thatcher (1999), Coseismic slip resolution along a plate boundary megathrust: The Nankai Trough, southwest Japan, *J. Geophys. Res.*, *104*, 1111–1129.

Sieh, K., and D. Natawidjaja (2000), Neotectonics of the Sumatran fault, Indonesia, *J. Geophys. Res.*, *105*(B12), 28,295–28,326.

Simoes, M., J. Avouac, R. Cattin, and P. Henry (2004), The Sumatra subduction zone: A case for a locked fault zone extending into the mantle, *J. Geophys. Res.*, *109*, B10402, doi:10.1029/2003JB002958.

Socquet, A., C. Vigny, N. Chamot-Rooke, W. Simons, C. Rangin, and B. Ambrosius (2006), India and Sunda plates motion and deformation along their boundary in Myanmar determined by GPS, *J. Geophys. Res.*, *111*, B05406, doi:10.1029/2005JB003877.

Steacy, S., J. Gomberg, and M. Cocco (2005), Introduction to special section: Stress transfer, earthquake triggering, and time-dependent seismic hazard, *J. Geophys. Res.*, *110*, B05S01, doi:10.1029/2005JB003692.

Stein, R. (1999), The role of stress transfer in earthquake occurence, *Nature*, *402*, 605–609.

Stein, R., and M. Lisowski (1983), The 1979 homestead valley eartquake sequence, california: Control of after-shocks and postsesismic deformation, *J. Geophys. Res.*, *88*, 6477–6490.

Townend, J., and M. D. Zoback (2004), Regional tectonic stress near the San Andreas fault in central and southern California, *Geophys. Res. Lett.*, *31*, L15S11, doi:10.1029/2003GL018918.

Vernant, P., and J. Chéry (2006), Low fault friction in Iran implies localized deformation for the Arabia-Eurasia collision zone, *Earth Planet. Sci. Lett.*, *246*, 197–206.

Vigny, C., A. Socquet, C. Rangin, N. Chamot-Rooke, M. Pubellier, M.-N. Bouin, G. Bertrand, and M. Becker (2003), Present-day crustal deformation around Sagaing fault, Myanmar, *J. Geophys. Res.*, *108*(B11), 2533, doi:10.1029/2002JB001999.

Vigny, C., et al. (2005), Insight into the 2004 Sumatra-Andaman earthquake from GPS measurements in southeast Asia, *Nature*, *436*, 201–206, doi:10.1038/nature03937.

Voisin, C., F. Cotton, and S. Di Carli (2004), A unified model for dynamic and static stress triggering of aftershocks, anti-shocks, remote seismicity, creep events, and multisegmented rupture, *J. Geophys. Res.*, *109*, B06304, doi:10.1029/2003JB002886.

Wessel, P., and W. Smith (1995), New version of the generic mapping tools released, *Eos Trans. AGU*, *76*(33), 329.